Chem Soc Rev

Photo-induced force microscopy (PiFM) - principles and implementations

Journal:	*Chemical Society Reviews*
Manuscript ID	CS-TRV-01-2022-000052.R1
Article Type:	Tutorial Review
Date Submitted by the Author:	31-Mar-2022

Complete List of Authors:	Sifat, Abid Anjum; University of California Irvine, Electrical Engineering & Computer Science Jahng, Junghoon; Korea Research Institute of Standards and Science, Hyperspectral Nano-imaging Lab Potma, Eric; University of California Irvine, Chemistry

Journal Name

ARTICLE TYPE

Cite this: DOI: 00.0000/xxxxxxxxxx

Photo-induced force microscopy (PiFM) - principles and implementations

Abid Anjum Sifat[a], Junghoon Jahng[b] and Eric O. Potma[a,c]

Received Date
Accepted Date

DOI: 00.0000/xxxxxxxxxx

Photo-induced force microscopy (PiFM) is a scan probe technique that offers images with spectroscopic contrast at a spatial resolution in the nanometer range. PiFM utilizes the non-propagating, enhanced near field at the apex of a sharp tip to locally induce a polarization in the sample, which in turn produces an additional force acting on the cantilevered tip. This photo-induced force, though in the pN range or less, can be extracted from the oscillation properties of the cantilever, thus enabling the generation of photo-induced force maps. Since its inception in 2010, the PiFM technique has grown into a useful nano-spectrocopic tool that has expanded its reach in terms of imaging capabilities and applications. In this review, we present various technical implementations of the PiFM approach. In addition, we discuss the physical origin of the PiFM signal, highlighting the contributions from dipole-dipole forces as well as forces that derive from photo-thermal processes.

Key Learning Points

- Photo-induced force microscopy (PiFM) is an imaging technique based on raster-scanning a sharp tip across the sample. When the tip is illuminated with light, it experiences an extra force due to the light-induced interactions between the sample and probe. This so-called photo-induced force constitutes the contrast mechanism in PiFM images.

- There are several physical mechanisms that play a part in the photo-induced force. For tip-sample distances in the (sub)-nanometer regime, the dominant forces are the electromagnetic gradient force and the thermally induced expansion force. Depending on the nature of the experiment and sample, either of these two forces can dominate the observed contrast.

- In PiFM imaging applications that involve thin films of organic materials under mid-infrared radiation, the thermal expansion force is found to be the dominant force. In PiFM applications that use visible light and nanoparticles with electronic resonances, the gradient force is often the dominant force.

1 Introduction

Driven by the need for spectroscopic sensitivity at the nanoscale, various forms of scan probe microscopy have been combined with light illumination strategies, resulting in a set of powerful techniques for generating nano-spectroscopic maps of materials and molecular samples. Photo-induced force microscopy (PiFM) is one of these approaches. Although based on principles that were already well understood, it was no sooner than 2010 when the first photo-induced force microscope was developed by Wickramasinghe and co-workers.[1] This first implementation of the PiFM principle produced images of clusters of molecular chromophores, where the force contrast appeared to result from the electronic transition of the dye molecules. The origin of the detected signal was attributed to the electromagnetic force between the dipolar charge oscillations in the illuminated tip and the induced polarization in the molecule. Since this force can, in principle, be sensed without physically touching the sample, this form of light-based scan probe microscopy differs from methods that require direct contact with the specimen. We will assign the PiFM label to those force-based, spectroscopic scan probe techniques that can be operated in non-contact mode.

PiFM is part of the larger family of nano-spectroscopic scan probe methods. Another important member of this family is apertureless (or scattering) scanning nearfield optical microscopy (a-SNOM or s-SNOM).[2] Like PiFM, sSNOM is a non-contact nano-imaging technique that derives contrast from a light-matter interaction in the sample. Unlike PiFM, sSNOM detects the light scattered from the tip-sample nanojunction in the far-field. Since the scattered light carries information about the induced polarization in the sample, sSNOM images exhibit spectroscopic contrast.

[a] Department of Electrical Engineering and Computer Science, University of California, Irvine, CA, USA.
[b] Hyperspectral Nano-imaging Lab, Korea Research Institute of Standards and Science, Daejeon 34113, South Korea
[c] Department of Chemistry, University of California, Irvine, CA, USA.; E-mail: epotma@uci.edu

Detecting such signatures against the general background of scattered laser light can be challenging. PiFM monitors the electromagnetic force rather than the scattered light, and, relative to sSNOM, can be considered a background-free technique.

Since the 2010 demonstration of PiFM, the method has been expanded from electronic resonances in the visible range to vibrational transitions in the mid-infrared range.[3–5] In addition, PiFM has also been used to probe nonlinear polarizations in the sample, resulting in images based on stimulated Raman transitions[6] and pump-probe transitions[7,8]. Along with the development of improved detection strategies[9–11], a great deal of progress has been made on the theoretical description of the PiFM signal[12–15], putting the PiFM technique on a more solid footing. Whereas the first applications of PiFM involved inorganic materials[1,16] and metals[17], the technique has since been used to study organic compounds (polymers[18] and organic semiconductors[19]), biological samples (collagen fibres[20] and protein structures[21]), as well as samples of geological significance (biominerals)[22].

The key component of the photo-induced force microscope is the oscillating tip-cantilever system that scans over the sample while it is illuminated. The cantilever oscillation frequencies are high, typically in the 100 kHz - 5 MHz range, similar to the situation in dynamic atomic force microscopy (AFM). The PiFM signal is based on the changes in the cantilever oscillation dynamics caused by the presence of the light field. To extract the photo-induced changes from other effects that influence the cantilever motion, the light field is modulated at a characteristic frequency f_m. In the most common implementation, the PiFM signal is derived from changes seen in the cantilever's amplitude at fixed f_m or another combination frequency that depends on f_m. This approach is referred to as amplitude modulation (AM)-PiFM. In another implementation the signal is extracted from the frequency modulation (FM) of the cantilever resonance, a method known as FM-PiFM.[9,10]

Although the PiFM experiment can be conducted in non-contact mode, in some cases it is carried out in tapping-mode, which produces stronger signals.[1,23]An alternative approach is to actively control the tip-sample distance by modulating the sample stage in tapping mode, while the cantilever itself is not actively driven. The PiFM signal is then obtained by illuminating the tip-sample junction with a pulsed source that is synchronized to the periodic modulation of the stage, altering the forces on the tip at a specific tip-sample distance.[5,24–26] This technique is referred to as peak force (PF)-PiFM, where the laser pulse is typically illuminating the sample moments before tip-sample contact.[3,11]

Upon light illumination, material properties like the polarizabilty (α) at the microscopic scale, or the permittivity (ε) and refractive index (n) at the macroscopic scale, dictate the sample's response. There are several mechanisms that can contribute to the force felt by the tip as a consequence of the presence of light. One mechanism is based on the induced charge oscillations in the tip and their interaction with the sample, and such interactions are enhanced near an optical resonance of the sample. The magnitude of the detected force changes as the excitation frequency is scanned over the optical resonance, rendering the PiFM signal spectroscopically sensitive. However, the spectral dependence of the photo-induced force depends on the product of the complex polarizabilities of the tip and the sample, which in most cases results in a dispersive lineshape.[12,13] Another mechanism that leads to detectable forces originates from the absorption of energy from the light field, part of which increases the temperature of the sample. The thermal expansion of the material that follows can affect the PiFM signal in a variety of ways, including through the thermally modulated Van der Waals force[4,27] or the thermally induced photo-acoustic force.[14] The dissipation of optical energy gives rise to a non-dispersive lineshape of the spectrally-resolved force. Opto-mechanical damping of the cantilever motions is a related mechanism that also gives rise to non-dispersive lineshapes.[15] Which effect is dominant depends on the wavelength range, material properties and the details of the experiment.

In this review, we first highlight the principles of AM-PiFM, followed by a discussion on various signal detection strategies and other system level improvements. We then examine several models that explain the origin of the photo-induced force under different experimental conditions. We conclude with a summary of recent PiFM studies, with an emphasis on how the excitation wavelength and material properties determine which physical mechanism provides the dominant contribution to the measured PiFM signal.

2 Principle of PiFM operation

2.1 Layout of the photo-induced force microscope

In its most basic implementation, the PiFM system is a scan probe microscope based on tapping-mode atomic force microscopy (AFM).[28] Since the demonstration of PiFM in 2010[1], AM-PiFM is the most commonly used configuration of the technique, and the layout of the AM-PiFM microscope is sketched in Figure 1. The main component of the system is the cantilever beam which is equipped with a sharp tip. The latter is typically gold-coated to increase the polarizability of the tip's apex. The motions of the cantilever are measured with high precision by illuminating its backside with a laser beam (feedback laser), which is reflected off the cantilever's surface and detected with a quadrant photodiode. The sample is placed on a glass coverslip and is illuminated from below in an inverted microscope configuration, although side-on illumination schemes are also common. The tip is positioned in close proximity to the sample and externally driven by a dithering piezoelectric element to force an oscillatory motion of the cantilever beam. The driving frequency is chosen to coincide with the mechanical resonance of the cantilever. In many PiFM measurements, the second mechanical resonance of the cantilever at frequency f_2 is chosen for recording the topographic AFM signal, which implies that the driving frequency is tuned to f_2. The PiFM signal is then derived from the cantilever's motions at its first mechanical resonance at frequency f_1. In other PiFM systems the roles of the f_1 and f_2 frequency channels are reversed. For consistency, in the remainder of this review, we will refer to f_1 as the PiFM channel and to f_2 as the topography channel.

The incident light is amplitude modulated at f_m, which can be accomplished for instance with an acousto-optic modulator (AOM). The light is subsequently focused at the tip-sample nano-

junction with a high numerical aperture lens from below or with an off-axis parabolic mirror from the side. In the presence of photo-induced forces, the cantilever develops motions that depend on f_m, and these motions can be detected by analyzing the signal of the quadrant photodiode. In a typical configuration, a lock-in amplifier is used to demodulate the photodiode signal at pre-selected detection frequencies. To extract the photo-induced force in the AM-PiFM instrument, the demodulation frequency is tuned near f_1. There are two common detection modes: homodyne and heterodyne. In the homodyne detection mode, also known as the direct mode, f_m is adjusted to coincide with f_1, i.e. $f_m = f_1$. In this setting, the modulation of the incident light produces a force that is directly manifest at the first mechanical resonance of the cantilever. In the heterodyne detection mode, sometimes referred to as the sideband detection mode, the laser modulation is performed at the difference frequency ($f_m = |f_1 - f_2|$) or sum frequency ($f_m = |f_1 + f_2|$) of the cantilever resonance frequencies. Once again, the signal is demodulated near mechanical resonance frequency f_1, which now registers an optically induced force at a sideband of the second mechanical resonance, i.e. $f_1 = |f_2 \pm f_m|$. While the homodyne mode is sensitive to the photo-induced force itself, the heterodyne detection mode probes the gradient of the photo-induced force.[23,29]

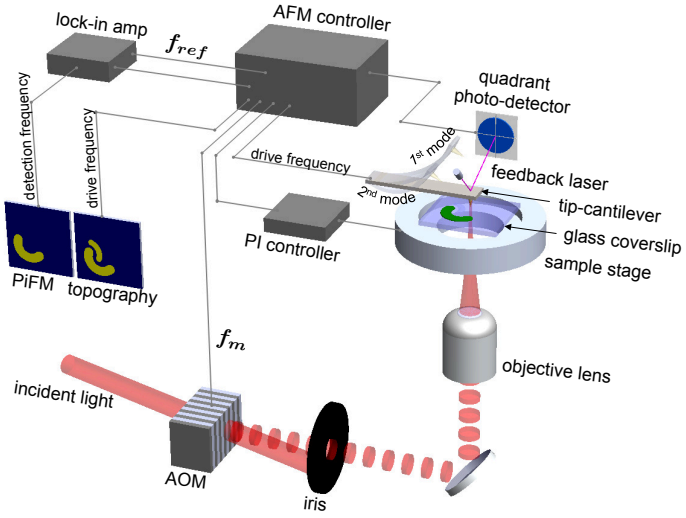

Fig. 1 Simplified schematics of AM-PiFM. AOM denotes the acoustic optic modulator, f_m is the modulation frequency, f_{ref} is the reference frequency of the lock-in amplifier that is the same as detection frequency.

2.2 Amplitude modulation and frequency modulation PiFM

In regular AM-AFM, while the cantilever deflection is recorded, a fixed tip-sample average distance is maintained through a proportional integral (PI) feedback controller that observes the amplitude changes at the driving frequency f_2. The feedback produces an error signal that is used to keep the amplitude constant at a pre-set value. Additionally, the topographic AFM signal is derived from the amplitude modulation found at f_2. Instead of monitoring the amplitude changes, it is also possible to perform the feedback by registering the changes in the cantilever's resonance frequency itself. The resonance frequency is a sensitive probe of the interactions between the sample and the cantilevered tip, and its shift is thus a measure of tip-sample distance. In frequency modulation (FM) feedback[30,31], the resonance frequency is kept constant, a mode of operation that is particularly useful under conditions of ultrahigh vacuum (UHV) when the mechanical resonances are very narrow. Some PiFM measurements under UHV conditions have been performed by using the FM mode for feedback.[9] Regardless of the method of feedback, most PiFM signals are obtained by detecting amplitude changes in the f_1 channel.

An example of an AM-PiFM system is depicted in Figure 2. The system uses the amplitude modulation principle for reading out the PiFM signal (at f_1). To detect the PiFM signal, the photodetector signal is demodulated by the lock-in amplifier using either $f_1 = f_m$ as the reference signal for homodyne detection or $f_1 = |f_2 \pm f_m|$ as the reference for heterodyne detection. The heterodyne detection mode is useful for enhancing the sensitivity to the gradient force by suppressing the contribution of the scattering force.[29] Because heterodyne detection samples the gradient of the force, it also reduces the relative contribution from constant thermal expansion forces.[9,27,32]

The FM method can also be used for reading out the PiFM signal.[10] In FM-PiFM, the change in drive frequency f_2, Δf signal, rather than the change in amplitude is used for extracting the heterodyne PiFM signal. In one implementation[10], the incident light is modulated at $f_m = 2f_2 + f_{ref}$ to get the frequency shift as $\Delta f = \Delta f(0) + \Delta f(f_{ref})$, where f_{ref} is the reference frequency of the lock-in, $\Delta f(0)$ is a fixed resonance frequency shift and $\Delta f(f_{ref})$ is the shift due to the PiFM response at f_{ref}.[10,33] To isolate the photo-induced force content, the Δf signal is demodulated at f_{ref} in a lock-in amplifier.[10]. Whereas AM-PiFM can operate under ambient conditions, UHV conditions are required for proper operation of FM-PiFM. Despite this additional requirement, FM-PiFM offers improved sensitivity compared to ambient AM-PiFM.

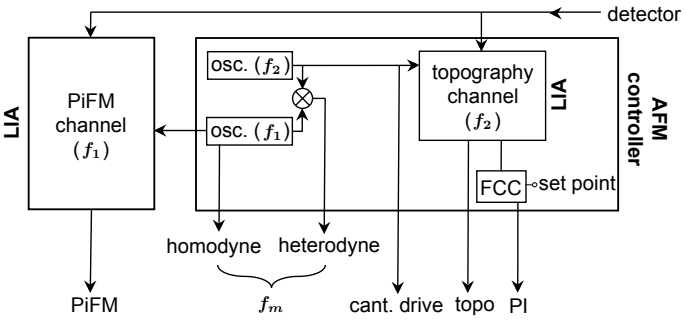

Fig. 2 Schematics of an AM-PiFM system. FCC: feedback control circuit; osc.: oscillator; LIA: lock-in amplifier.

2.3 Modulation strategies

The AOM is a common strategy to modulate the incident light in AM-PiFM measurements. However, it is also possible to use the intrinsic repetition rate of a pulsed laser as the source of modulation.[4] When using heterodyne detection in this configuration, the laser repetition rate must be tuned to $f_m = |f_2 \pm f_1|$, which is typically in the 100 kHz – 2 MHz range. Depending on the light source, it may be challenging to reach the required modulation

frequency, especially in the mid-infrared range where the repetition rate of quantum cascade lasers cannot be freely tuned into the >100 kHz range. In such cases, it is possible to dial down the modulation frequency by dividing $f_2 \pm f_1$ by an integer. This process of light modulation, called harmonic heterodyne detection[4], is shown in Figure 3(a) for the case of AM-PiFM. Another implementation uses modulation of the polarization orientation of the incident light pulses, a technique named sequential heterodyne detection schematically depicted in Figure 3(b). Here, the laser repetition rate is tuned to $f_2 \pm f_1 + f_p$, where f_p is the frequency of polarization modulation ($f_p \sim 40-200$kHz). The polarization modulation can be achieved with a photoelastic modulator (PEM), which switches the polarization periodically between a parallel alignment with the long axis of the tip and a perpendicular alignment in a side-on illumination configuration. Since only the parallel alignment of the polarization produces near field enhancement under the tip, this modulation scheme gives rise to an effective on/off switching of the near field illumination.

Furthermore, heterodyne detection can also be achieved when the light is modulated at $|f_2 \pm f_1|/2 + f_p$ and the PiFM signal is extracted at the f_1 detection mode.[4] The harmonic detection method has also been demonstrated for homodyne detection of the AM-PiFM signal.[34] It is interesting to note that by detecting the signal at higher harmonics of the modulation frequency, the effective time resolution of the PiFM measurement can be improved. This feature has been used to probe the dynamics of the cantilever, after the illumination is suddenly switched off, with a sub-μs temporal resolution. Such measurements are sensitive to the presence of forces that manifest themselves on the sub-μs timescale, which includes force dynamics due to the relaxation of the sample's thermal expansion. It was shown that the second harmonic of the modulation frequency, where the light is modulated at $f_m = f_1/2$ and the signal is detected in the $f_1 = 2f_m$ channel, is sufficient to improve the time resolution to better than 100 ns.[34]

2.4 Peak force PiFM

In standard AM-PiFM, the cantilever is driven into one of its mechanical resonances to collect the topography signal, and the presence of the photo-induced force is detected at another mechanical resonance of the cantilever. In PF-PiFM[11,24], the cantilever is not driven into one of its mechanical resonances. Instead, the sample stage position is periodically changed such that the tip-sample distance is actively modulated, a mode of operation referred to as peak force tapping (PFT) mode.[35] Figure 4(a) shows the photo-detector signal during the PFT cycle. In a typical PFT cycle, the cantilever deflection amplitude decreases when the tip is brought in closer proximity to the sample due to the increasing attractive tip-sample interaction force. At a certain distance, the tip starts to feel the repulsive side of the interaction potential, and full contact is reached as the sample position is increased further during the approach part of the PFT cycle. The trend is repeated in reverse during the retraction phase of the cycle.

When the arrival of the laser illumination pulse in the tip-sample junction is synchronized with the periodic modulation in

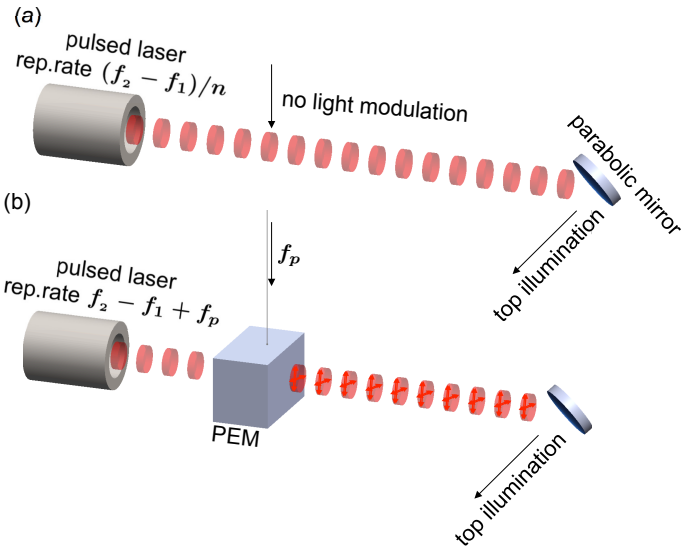

Fig. 3 Illumination scheme of (a) harmonic heterodyne and (b) sequential heterodyne detection PiFM. PEM: photo elastic modulator.There is no external light modulation in (a), the repetition of the pulsed laser itself provides the necessary modulation.

PFT mode, the time-delay in the synchronization loop allows the precise timing of the light pulse relative to the tip-sample distance. Applying the laser pulse at the moment of tip-sample contact, as shown in Figure 4(a), allows a measurement of the effect of thermally induced expansion forces near the contact resonance. The light-induced changes to the PFT cycle reveal the dynamics of thermal expansion and its subsequent relaxation. Since the magnitude of the thermal component depends on the laser wavelength and the absorption properties of the sample, scanning the illumination wavelength allows the recording of the sample's absorption spectrum. This recipe has been successfully applied in the mid-infrared, producing spectra that resemble spectra obtained through Fourier transform infrared (FTIR) spectroscopy. This detection modality is called peak force infrared microscopy (PFIR).[24] The technique is related to photothermal infrared resonance (PTIR) microscopy[36,37], but it has the added advantage of reducing tentative mechanical damage to the sample sustained during the contact resonance.

In its original implementation, PFIR uses a single laser pulse per PFT cycle of PFIR. Further sensitivity can be attained by introducing multiple pulses per PFT cycle.[25] If the time separation between the pulses in the multi-pulse burst is chosen to coincide with the oscillation period of the cantilever contact resonance, then the coherent sum of the light-induced signals in the PFT cycle provides an additional increase of the PFIR signal. Multi-pulse PFIR has also been combined with total internal reflection (TIR) illumination[38], in which case the stage is fixed and tapping is achieved by moving the cantilever instead. Excitation with TIR provides higher field enhancement than in side-on illumination[38] and has been used for PFIR studies in the liquid phase.[5,26]

Finally, the photo-induced response can be probed by timing the arrival of the laser pulse in the tip-sample non-contact zone, right before the moment of jump-to-contact.[3] This scenario is illustrated in Figure 4(b). This is the PF-PiFM method, which

has been applied to mid-infrared nanoscopy studies. The PF-PiFM spectra retrieved from polymer samples were shown to mimic those recorded with FTIR spectroscopy. Unlike the PFIR approach, the PF-PiFM technique is, in principle, a non-contact method and can thus be classified under the general umbrella of PiFM techniques.

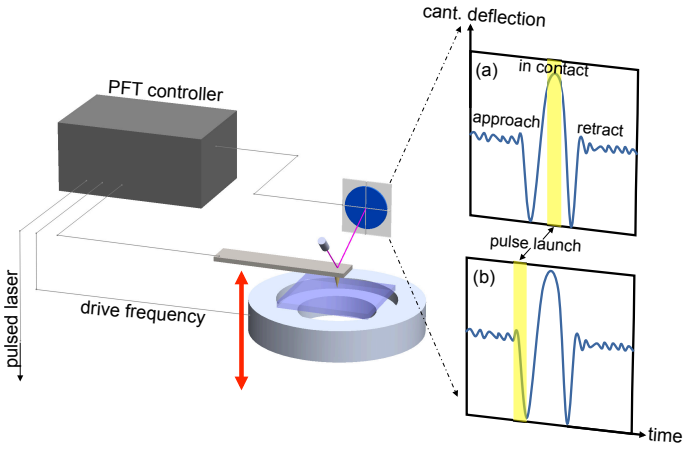

Fig. 4 Major distinction of peak force tapping mode PFIR and PF-PiFM from conventional tapping mode PIFM. The trend of PFT cycle and laser pulse launching time for (a) PFIR microscopy and (b) PF-PiFM system.

3 Physical origin of the photo-induced force

The physics of the illuminated tip-sample junction is complicated, and it comes as no surprise that the detected forces in PiFM derive from various mechanisms. Originally conceived for probing the instantaneous electromagnetic force between the tip and the sample[1,39], it has become clear that other contributions to the force play a role as well. Depending on the geometry of the experiment, wavelength setting and properties of the material, the instantaneous electromagnetic force may be inferior to other photo-induced forces. Chiefly among these are forces that are derived from light absorption by the sample or tip, and the thermal expansion of the sample that follows.[3,12,14,15,27] In this Section, we discuss various contributions to the force that can be manifest in a PiFM experiment.

3.1 Photo-induced electromagnetic force

When the cantilevered tip is illuminated, charge oscillations in the tip's material produce an induced polarization at the optical driving frequency. In most cases, this polarization can be approximated well as an oscillating dipole in the form $p_t = \alpha_t E$, where $\alpha_t = \alpha_t' + i\alpha_t''$ is the polarizability of the tip and E is the optical driving field. For simplicity, we will assume that the polarizability is a scalar quantity. The oscillating dipole experiences a time-averaged, electromagnetic force that is proportional to the gradient of the driving field as follows:

$$\langle F \rangle = \frac{\alpha_t'}{2} \sum_i \mathrm{Re}\{E_i^* \nabla E_i\} + \frac{\alpha_t''}{2} \sum_i \mathrm{Im}\{E_i^* \nabla E_i\} \qquad (1)$$

where $i = \{x, y, z\}$ labels the Cartesian components. The first term in equation (1) is proportional to the real part of the tip's polarizability, and is a non-dissipative, conservative force.[23,39] This term is related to the so-called gradient force. The second term in equation (1) is a dissipative, non-conservative force, which is proportional to the imaginary part of α_t. This force is related to the transfer of momentum of the scattered light and is called the scattering force.[39]

The first term in particular is sensitive to the gradient of the optical field in the vicinity of the tip. A steeper gradient produces a stronger force. For instance, the force can be expected to be strong when the tip is placed near the strong local fields associated with surface plasmon resonances, which show a significant spatial dependence on the nanoscale and thus exhibit non-negligible gradients. Indeed, this mechanism is responsible for the PiFM contrast observed near interfaces that support surface plasmon polaritons[40] or objects that display localized surface plasmons.[17,34] In the same fashion, PiFM is sensitive to the fields on the surface of materials that support collective modes such as phonon polaritons.[41,42]

The details of the local field also change when the tip is brought into close proximity to the surface of dielectric substrates or objects, which in turn alters the photo-induced force. The resulting force can be modeled conveniently with image dipole theory as illustrated in Figure 5(a). Writing the image dipole as $p_{t'}$ with polarizability $\alpha_{t'}$, and assuming that the dominant polarization direction is along z, the distance-dependence force directed along the z-axis can be expressed as[23]:

$$\langle F_g \rangle_z \simeq -\frac{3\mathrm{Re}\{\alpha_t \alpha_{t'}^*\}}{4\pi\varepsilon_0\varepsilon_m z^4} |E_z|^2 \qquad (2)$$

where ε_m is the permittivity of the medium surrounding the tip. This force, which we will refer to as the gradient force, explicitly depends on the distance z between the tip and image dipoles, and scales as z^{-4}. Therefore, the optical gradient force is strongest when the tip-sample distance is small, whereas it falls off quickly when the tip is retracted. The negative sign indicates that the force is attractive. Since the magnitude of the image dipole depends on the permittivity of the substrate material, the magnitude of the photo-induced force felt by the tip is sensitive to the properties of the material underneath it.

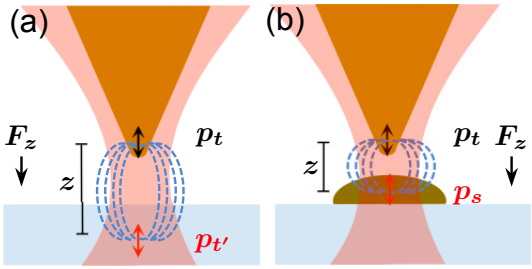

Fig. 5 Illustration of (a) the image dipole force above the substrate, and (b) the dipole-dipole interaction force between tip and sample. z is the average distance of the tip dipole p_t from the image dipoles p_t' in (a), and from the sample dipole p_s in (b)

3.2 Dipole-dipole interaction force

Consider a small object, such as a cluster of molecules, that is illuminated by a focused light field. At the microscopic level the induced polarization of the sample is $p_s = \alpha_s E$, where $\alpha_s = \alpha_s' + i\alpha_s''$ is the polarizability of the sample. The real and imaginary parts of the polarizability are shown in Figure 6 near a single optical resonance of the sample.

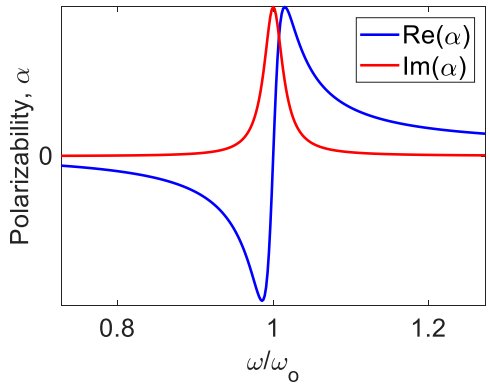

Fig. 6 Typical spectral behavior of the real and imaginary parts of the polarizability near an optical resonance (resonant frequency=ω_o) of a molecular material.

The presence of p_s affects the local field near the induced dipole of the tip and thus has an effect on the electromagnetic force exerted on the tip.[13] Figure 5(b) shows a schematic of the interaction between the oscillating dipoles as mediated by the local electromagnetic field. This interaction is sometimes called the dipole-dipole force, and the time averaged dipole-dipole gradient force can be written as:

$$\langle F_g \rangle_z \simeq -\frac{3\mathrm{Re}\{\alpha_t \alpha_s^*\}}{4\pi\varepsilon_0\varepsilon_m z^4}|E_z|^2 \qquad (3)$$

which also displays a z^{-4} dependence. The spectral response is proportional to $\mathrm{Re}\{\alpha_t \alpha_s^*\} \propto \{\alpha_t'\alpha_s' + \alpha_t''\alpha_s''\}$. For a typical metal, $\alpha_t' \gg \alpha_t''$ over the visible to infrared spectral range.[12] Under these conditions, the spectral response for the dipole-dipole gradient force assumes a characteristic dispersive lineshape. The presence of a dispersive lineshape in the photo-induced force near an optical resonance is thus an indication that the dipole-dipole force is a prominent contribution to the PiFM measurement. Calculations show that the optical gradient force that can be expected between the tip and a small nanometer-sized structure, such as a molecular cluster or quantum dot, is on the order of a pN.[13] Though small, such forces can still be measured with confidence in the PiFM microscope.

Note that a spectral resonance is not a prerequisite for observing contrast in PiFM through the dipole-dipole interaction force. Since the PiFM signal is governed predominantly by the magnitude of $\alpha_t'\alpha_s'$, any changes in the real part of the material's polarizability across a spatially heterogeneous sample can give rise to contrast in the PiFM map. For this reason, PiFM imaging can be used to study samples with a spatially varying refractive index using excitation light that is off-resonant with optical transitions in the sample material.[32,43]

3.3 Photo-thermal expansion force

Photo-thermal expansion forces follow from the sample expansion after light absorption, shown schematically in Figure 7(a). The thermal expansion ΔL of the sample is related to the rise in temperature, ΔT, at the location of laser illumination. The expansion can be modeled as $\Delta L \approx \alpha_T h \Delta T$, where h is the sample thickness and α_T is the linear thermal expansion coefficient of the sample.[27,37,44] ΔT can be obtained by solving heat equation with the incident light power as the heat source.[27,37] Note that the photo-thermal expansion is a direct function of the sample thickness whereas the dipole-dipole interaction force is virtually insensitive to h.[14] For organic materials in the $h \sim 1-100$ nm range the material expansion is typically very small, on the order of $\Delta L \sim 1-100$ pm, which is often smaller than the size of an atom! Nonetheless, such height variations can still be detected

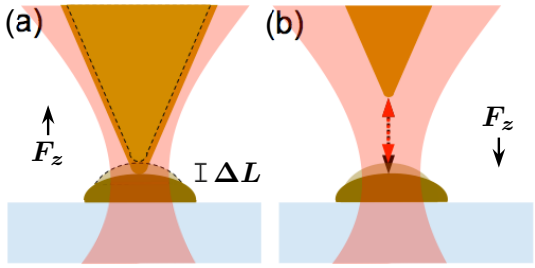

Fig. 7 Sketch of (a) the thermal expansion force in contact mode, and (b) the thermally modulated van der Waals force contribution in non-contact PiFM. Modulation of the incident light produces a modulation in tip-sample distance, ΔL. This in turn results in modulation of van der Waals force (black arrow to red arrow) at f_m.

through changes in the force. In general, even in the absence of light, the tip experiences an interaction force due to its proximity to the sample. This tip-sample interaction force, $F_{ts}(z)$, is described well as the sum of conservative and non-conservative forces given by $F_{ts}(z) = F_c(z) - \Gamma(z)\dot{z}$, where F_c is the conservative force and $\Gamma(z)$ represents an effective damping coefficient of a given dissapative process.[23,29] The F_{ts} strongly depends on the tip-sample distance and contains attractive and repulsive contributions. Figure 8 shows F_{ts} as a function of z. In the non-contact zone, F_{ts} is dominated by attractive forces, such as the van der Waals (vdW) force, whereas in the contact zone repulsive forces become the dominant force. At $z = 0$ and shorter distances the tip is in full contact with the sample and F_{ts} is exclusively repulsive. Such forces are described well by the Derjaguin–Muller–Toporov (DMT) model. Both vdW force and the DMT force depend on z. Sample expansion causes a change in the tip-sample distance, and thus produces a difference in the force:

$$\Delta F_{ts}(z) = F_{ts}(z - \Delta L) - F_{ts}(z) \qquad (4)$$

The effect of the light-induced sample expansion is given by the dashed red curve in Figure 8, which emphasizes that there is a periodic force difference due to a periodic modulation of the light, both in the contact and non-contact zones. In the small oscillation limit, the tip-sample force can be expanded in a Taylor series around the average position z_c, which in the first-order approxi-

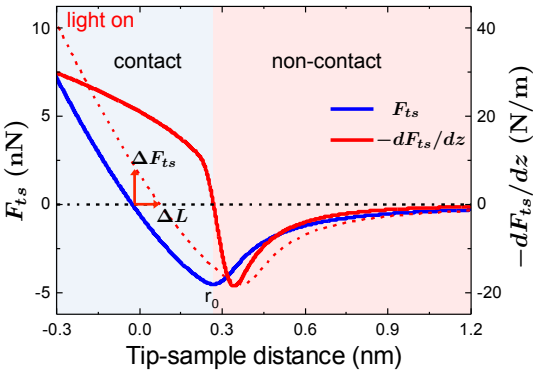

Fig. 8 Effect of the thermal expansion ΔL on the tip-sample interaction force F_{ts}. Blue curve shows F_{ts} when the light is off, while red dashed curve shows F_{ts} when the light is on. Red solid curve shows -$\partial F_{ts}/\partial z$, which is proportional to the magnitude of the thermal expansion force.

mation takes on the form:

$$F_{ts} \approx F_{ts}(z_c) + \frac{\partial F_{ts}}{\partial z}(z - z_c) + \ldots \tag{5}$$

so that the force difference can be generally expressed as:

$$\Delta F_{ts}(z) \approx -\frac{\partial F_{ts}}{\partial z}\Delta L \tag{6}$$

The magnitude of the force difference is thus related to the spatial derivative of the tip-sample force, shown by the red curve in Figure 8. In the contact zone, using a DMT model for F_{ts}, the thermal expansion force F_{th} can be written as:[44]

$$F_{th}(z) = \Delta F_{ts}(z) \approx 2\mathrm{E}^* \sqrt{R(r_o - z)} \cdot \Delta L = C(z) \cdot \Delta L \tag{7}$$

where E^* is the reduced Young's modulus of the material, R is the radius of the tip, r_o is the intermolecular distance in the material and $r_o - z$ is the indentation depth. The repulsive expansion force depends linearly on ΔL. Since ΔL is modulated at f_m in a PiFM experiment, the repulsive force F_{th} shows up as PiFM signal when operated in contact mode. Even for small ΔL, F_{th} can be significant. For instance, for molecular monolayers, a value for $C(z)$ as high as ~ 40 N/m has been reported, so that the force measures 130 pN for a sample expansion of only 3.2 pm.[44] Since the photothermal response depends on the absorption of the sample, the force spectrum follows the dissipative part of the material response, resulting in a non-dispersive resonance lineshape.

3.4 Thermally modulated van der Waals force

The discussion in the previous section makes it clear that the thermal expansion also gives rise to a modulation of the tip-sample force in the non-contact zone[32], shown schematically in Figure 7(b). Assuming that the force in this zone is described well by the attractive vdW force, the photoinduced thermal expansion force can be obtained from equation (6) as:

$$F_{th}(z) \approx -\frac{H_{\mathrm{eff}} R}{6}\frac{1}{z^3}\Delta L \tag{8}$$

where H_{eff} is the effective Hamaker constant between the tip and the sample. We will refer to this force in the non-contact zone as the thermally modulated vdW force.

The thermal expansion of the sample can be split into two parts and written as $\Delta L_{tot}(z) = \Delta L_t(z) + \Delta L_d$. Here ΔL_d is the thermal expansion due to the total illuminated sample volume, which is independent of the tip-sample distance. The thermal expansion due to the heating right underneath the tip is described by $\Delta L_t(z)$, which relies on the field enhancement in the tip-sample junction and thus depends on the tip-sample distance.[27] Figure 9(a) shows the calculated thermal expansion of a polystyrene(PS) layer while it is illuminated with 1452 cm^{-1} light that is on-resonance with a vibrational mode in PS. For ΔL_d the heated volume is calculated from the beam radius and sample thickness, whereas for $\Delta L_t(z)$ the heated volume is related to the thermal diffusion length l_p of the sample material.[27,32] For a laser pulse duration of τ_p, the diffusion length is defined as $l_p \sim \sqrt{D\tau_p}$, where D is the thermal diffusivity of the sample.[27,45] While the direct thermal expansion ΔL_d is linearly proportional to the sample thickness L up to the beam radius, the tip-enhanced thermal expansion reaches a near constant value after a certain sample thickness, which is related to l_p.[27]

The direct and tip-enhanced thermal expansion are both modulated at f_m, and thus can be detected in the homodyne detection mode. Since the direct thermal expansion is independent of the tip position, it does not show up in the heterodyne mode. The tip-enhanced expansion, however, depends strongly on tip-position and is, therefore, manifested in the heterodyne detection channel. For this reason, the tip-enhanced expansion can be exclusively detected in a heterodyne PiFM experiment.

Although the tapping mode PiFM can contain contributions from both the contact mode and the non-contact mode of operation, such PiFM experiments are typically conducted in the attractive force region to avoid tip damage. In this case, the experiment is more sensitive to the thermal modulation of the attractive vdW force.[27] On the contrary, PTIR measurements[36,37,46] are predominantly sensitive to the thermal modulation of the repulsive DMT contact force as in equation (7). Because the tip is in contact with the sample without active oscillation (no tip-sample distance change), the total thermal expansion is directly manifested at the light modulation frequency of f_m, which rises monotonically as a function of sample thickness as shown in Fig. 9(a).[27,47] Figure 9 (b) shows PiFM and PTIR measurements on a polystyrene wedge atop a Si substrate. On vibrational resonance, the heterodyne PiFM signal tracks ΔL_t, while the PTIR signal shows the gradually increasing response with sample thickness that is characteristic for the behavior of L_{tot}.

3.5 Thermally induced photo-acoustic force

The photothermal expansion and subsequent relaxation of the sample can be accompanied by a longitudinal acoustic wave that results from the periodic compression and decompression of the material. Because the acoustic wave travels in the material medium at a higher speed than its corresponding propagation speed in air, a shock wave forms at the sample/air interface, which subsequently travels through the air medium. Impulsive thermal expansion can create shock waves that are capable of pro-

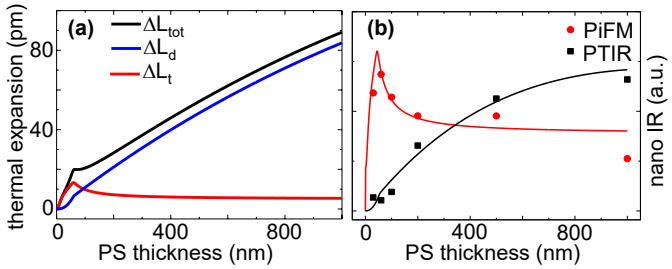

Fig. 9 (a) Calculated thermal expansion for a polystyrene (PS) film of varying thickness on Si substrate at 1452 cm^{-1}, showing direct thermal expansion (blue), tip-enhanced thermal expansion (red) and total thermal expansion (black). (b) Thickness dependence of PiFM and PTIR signal at the 1494 cm^{-1} vibrational resonance of PS. Squares and dots represent the measured data and solid line is the theoretically fitted curve. Reprinted (adapted) with permission from [27]. Copyright 2018 American Chemical Society

viding an upward push to the tip-cantilever system in the sample's vicinity.[14] Note that the photo-acoustic effect is zero in vacuum.

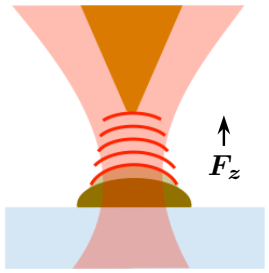

Fig. 10 Thermally induced photo-acoustic force on the tip in non-contact PiFM. The red lines depict the air compression upon acoustic shock wave propagation.

A schematic of this phenomenon is presented in Figure 10. The acoustic shock wave generates a spatial variation in the air pressure in the tip-sample junction. The energy carried by such an acoustic wave for a $1-10$ pm thermal expansion is on the order of a few femto-Joules, which is comparable to the oscillation energy of a cantilever that has an oscillation amplitude of tens of nanometers.[14] In principle, energy exchange between the acoustic wave and the cantilever is possible, and it is most significant over distances shorter than the mean free path of air molecules, about 70 nm. Since it depends on the thermal expansion of the sample, the photo-acoustic effect is proportional to sample thickness. Note that the decay of the acoustic wave away from the surface is generally much slower than the steep power law dependence of the optical gradient force and other tip-sample interaction force like the vdW force. For this reason, the photo-acoustic force can be present as a background that is nearly constant with tip-sample distance, on top of which other force contributions with steeper distance dependencies are manifest.[15]

3.6 photo-induced damping of the cantilever

As state above, $F_{ts}(z)$ is described well as the sum of conservative and non-conservative force. The vdW force and the DMT force are the examplar attractive and repulsive conservative forces. Unlike conservative forces, non-conservative forces dissipate mechanical energy into other forms of energy, which includes energy exchange between the cantilever and the sample. The separation of the interaction force into conservative and non-conservative forces is helpful for examining their effects on the cantilever motions. For instance, changes in the cantilever's spring constant k due to tip-sample interactions are related to conservative forces as $k_i' = k_i - \frac{\partial \overline{F_c}}{\partial z}$, where i denotes the cantilever mode and $\overline{F_c} = F_c + F_{pif}^{DC}$. Here, F_{pif}^{DC} includes any DC component of the photo-induced force. On the other hand, changes to the cantilever's damping coefficient are mediated by the non-conservative forces in the form $b_i' = b_i + \Gamma(z_c)$.[29]

As shown in Figure 11(a), the change in spring constant due to the conservative force shifts the resonant frequency of the cantilever oscillation. Any net attractive interaction force tends to shift the resonant frequency toward lower frequencies, while repulsive forces shifts the resonance to higher frequencies.[15,27,29,48] Conversely, the damping coefficient does not affect the resonant frequency, but it rather lowers the quality factor of the oscillator. This is illustrated in Figure 11 (b), where the rise in b decreases the oscillation amplitude.[15] Non-conservative forces that can cause changes in b include velocity dependent adhesion and viscoelastic forces in contact mode, and tip heating[48] or the effects of radiation pressure in non-contact mode. In the case of photothermal expansion forces, ΔL can modulate the conservative and non-conservative tip-sample interaction forces, and can therefore modulate the spring constant k or the damping coefficient b.[15]

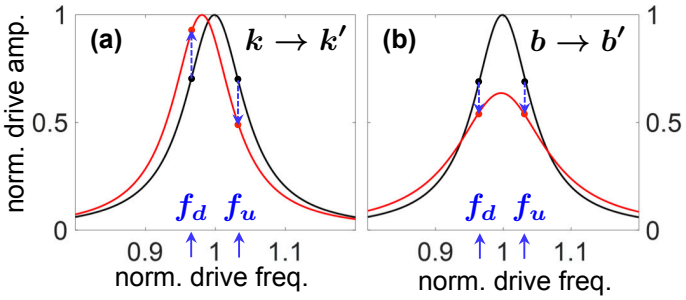

Fig. 11 Cantilever oscillation amplitude near resonance. Free oscillation response is shown by the black line, while the red line indicates response in case of an externally applied force. (a) Resonant frequency shift due to modulation of the spring constant. (b) Amplitude change due to damping. f_d and f_u indicate two observation frequencies down-shifted or up-shifted from the resonance frequency of the free oscillation.

A defining feature of photo-induced damping of cantilever motions can be observed by monitoring the oscillation amplitude at two observation frequencies, one up-shifted (f_u) from the resonance frequency and another one down-shifted (f_d), as shown in Figure 11(b). Damping alters the overall amplitude of the resonance curve, which means that the amplitude measured at f_u and f_d are the same. This is in contrast with the effect of a changing spring constant, in which case the amplitude measured at f_u is higher than at f_d for an increasing spring constant. Switching the observation frequency between f_u and f_d gives rise to a clear modulation of the signal for changes to k, while no such modula-

tion is observed for changes mediated via b.

When the conservative forces are not significantly changing in the experiment, PiFM contrast due to changes in b can become important. In this case, the PiFM spectrum would follow a dissipative lineshape, similar to the lineshape expected for thermal expansion forces. In fact, the photo-induced damping principle has been suggested as an alternative mechanism to thermal expansion for explaining the observed dissipative spectral profiles in PiFM measurements performed in the infrared range.[15].

4 Photo-induced force microscopy in practice

The different mechanisms discussed in the previous Sections can all play a role in the measured PiFM signal. Which effect dominates depends on the properties of the material and the details of the experiment. Dipole-dipole forces between the illuminated sample and the tip are generally weak but can be expected to dominate in case of strongly polarizable objects. Cases in which the electromagnetic force in PiFM is the dominant contribution to the signal are found for nano-particles with strong electronic resonances, such as clusters of dye molecules or metallic particles with surface plasmon resonances. An example is given in Figure 12(a), which shows the spectral dependence of the PiFM signal for a cluster of silicon naphthalocyanine molecules. The PiFM signal follows the real part of the polarizability, which is a strong indication that the PiFM response is dictated by the instantaneous electromagnetic force.

The photothermal force F_{th} is always present, but is expected to be negligible for very thin samples in non-contact mode. In the case of molecular samples thinner than ~ 10 nm, the photothermal signal is typically very weak. For thicker samples, the thermal expansion grows and can dominate the PiFM signal. This situation is relevant for PiFM measurements in the mid-IR range, which are often performed on material layers of thickness 100 nm or higher. An example is shown in Figure 12(b), which depicts the PiFM response near the carbonyl (C=O) vibrational resonance for a layer of polymethyl methacrylate (PMMA), revealing a characteristic dissipative lineshape.

Several experimental observables can help determine whether the forces in given PiFM experiment are dominated by direct electromagnetic interactions or by indirect thermal effects. Based on the discussions above, the following features of the force signal are relevant:

- *Spectral dependence near an optical resonance of the material*. The electromagnetic force invariably follows a dispersive lineshape, whereas thermal effects are characterized by dissipative lineshapes.

- *Tip-sample distance dependence*. The optical gradient force falls off quickly as z^{-4}, while thermal effects like the modulated vdW force ($\propto z^{-3}$) or photo-acoustic forces show a shallower dependence on the tip-sample distance.

- *Dependence on sample thickness*. Thermal effects grow with the illuminated sample volume and thus increase with the sample's thickness, whereas the optical gradient force is nearly insensitive to the sample's thickness beyond the first molecular layers.

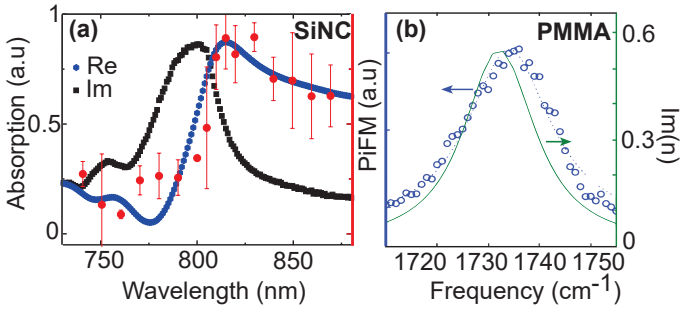

Fig. 12 (a) Measured PiFM spectrum (red dots) for a SiNC nanocluster and the extracted real (blue) and imaginary (black) parts of the SiNc response near the peak absorption at 810 nm. Reprinted (adapted) with permission from[16]. Copyright 2015 American Chemical Society. (b) PiFM spectrum measured (blue dots) for PMMA compared to the calculated imaginary part (green curve) of the refractive index of PMMA near the carbonyl (C=O) resonance of 1735 cm^{-1}. Reprinted (adapted) with permission from[14]. Copyright 2018 American Chemical Society.

In the following, we will discuss various practical situations under which either the electromagnetic force or thermal effects are dominant in the PiFM experiment.

4.1 Electromagnetic forces in PiFM

Clusters of molecular chromophores with resonances in the visible frequency range, as well as metal and dielectric nanostructures like nano-antennas, nano-clusters and quantum dots (QDs) with strong electronic resonances, are characterized by effective polarizabilies that are high enough for raising the electromagnetic force in PiFM above the noise floor. The first PiFM report focused on clusters of 6-tamra dye molecules, as shown in Figure 13. When excited near resonance at 543 nm, the PiFM map showed clusters, whereas no such features were observed when the laser excitation wavelength was tuned away from resonance.[1]

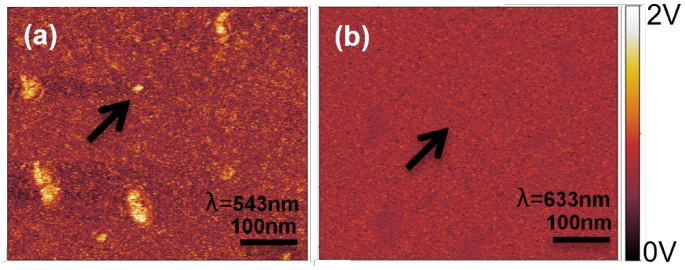

Fig. 13 PiFM image of 6-tamra dye molecular clusters on glass measured (a) on-resonance and (b) off-resonance with the 543 nm electronic transition. The black arrow in panel (b) points to the same location as in panel (a). Reprinted with permission from ref[1] © AIP Publishing.

The induced polarization of semiconducting nanostructures with bandgap energies in the visible or near-infrared can also be strong enough under typical PiFM experimental conditions to produce a detectable optical gradient force. An example is shown in Figure 14(a), where a dumbbell-shaped Zn–Ag–In–S nanostruc-

ture is subjected to PiFM examination.[33] The bandgap energy of this structure is position dependent and measures 1.97 eV at its bulbous extremities and 2.92 eV near its much narrower neck. Figure 14(b) shows the PiFM image taken at 660 nm (1.88 eV), near-resonant with the ends of the dumbbell structure but off-resonant with the middle part of the object. As expected, the signal is strongest at the ends of the nano-object. This measurement was performed in the heterodyne FM-PiFM mode, which offers high sensitivity to the optical gradient force and thus reduces thermal contributions to the PiFM measurememt.

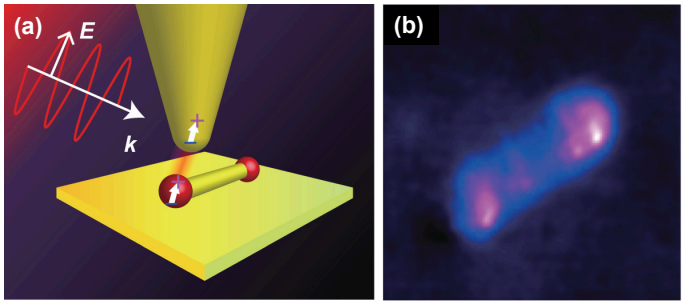

Fig. 14 PiFM imaging of Zn–Ag–In–S semiconducting nanostructures. (a) Schematic of the experimental layout. (b) PiFM image of the nano-object. Image was taken in heterodyne FM-PiFM mode, which offers exquiste senstivity to the optical gradient force. Reprinted with permission from ref[33] Copyright © 2021.

A strong response in the mid-infrared range can also give rise to detectable electromagetic photo-induced forces. An example is shown in Figure 15, which depicts results obtained from a study on 100 nm thick ribbons of InAsSb, a highly doped semiconducting (HDS) nanostructure that behaves as an epsilon near zero (ENZ) material near its plasma frequency, a spectral region where a strong mid-infrared response can be expected.[49] The PiFM signal in the vicinity of this structure can be modeled by calculating the effective polarizability of the tip in the dipole approximation, and by taking into account the scattered field from the HDS nanostructure. Based on the dielectric function of this HDS material, low PiFM signals are expected in the ENZ spectral range near $\sim 9\ \mu$m and a maximum is predicted toward lower energies, as shown by the gray line in Figure 15(a). The experimental data, shown in blue, follows the dispersive lineshape that is characteristic of the electromagentic force. PiFM images, taken at 9.02 μm and 10.53 μm, are shown in panels (b) and (c), respectively. Unlike mid-infrared near field studies on thin films with polariton modes near the ENZ region,[50] the measured PiFM signal here is fully explained in terms of the time-averaged electromagentic force without a significant contribution from thermal expansion forces.

A prime example of a strong collective excitation is found in the localized surface plasmon modes of metallic nano-structures. Figure 16(b) shows a PiFM map of a 100 nm Ag nano-particle.[34] The contrast is based on the strong fields associated with the plasmon mode which have steep gradients and can thus be measured directly through the optical gradient force. As expected, the PiFM response is strongest at the particle's interface in the direction of the incident polarization, which corresponds to the spatial distribution of the enhanced local field. Although illumination of the particle inevitably leads to photothermal heating of the lattice, thermal expansion effects are inferior to the electromagnetic photo-induced force in this case. Because of the high thermal diffusivity constant of silver, heat produced due to the optical excitation is distributed throughout the lattice on the sub-ns timescale, much faster than the modulation cycle. Thermal expansion forces would thus appear at all locations of the tip over the particle's surface. Given that the PiFM signal is negligible for most of the particle's surface, thermal expansion forces do not contribute to this measurement in a significant way.

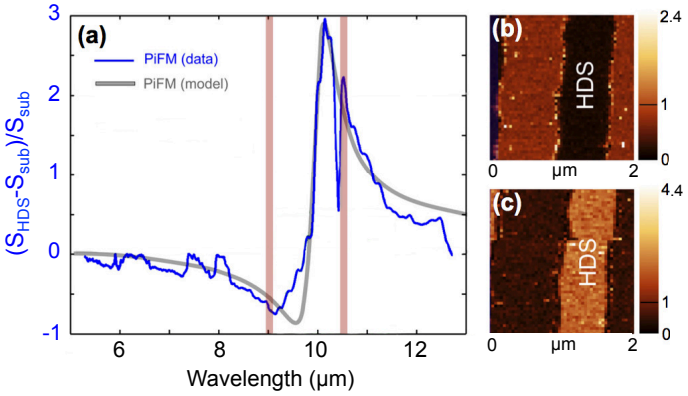

Fig. 15 PiFM imaging of an epsilon near zero (ENZ) material in the mid-infrared range. (a) Spectral dependence of the PiFM signal S_{HDS} in the mid-infrared range. Vertical bars show the spectral postion at which the images shown in (b) and (c) are taken, corresponding to 9.02 μm and 10.53 μm, respectively. Reprinted with permission from ref[49] Copyright © 2018.

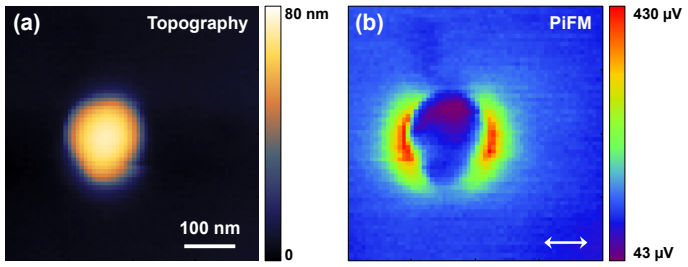

Fig. 16 PiFM imaging of a localized surface plasmon mode of metallic nano-particles. (a) Topographic image of a 100 nm diameter silver nano-particle. (b) PiFM image obtained with a 809 nm laser beam polarized in the direction of the white arrow. Reprinted with permission from ref[34] Copyright © 2021.

4.2 Thermal effects in PiFM

Thermal effects are expected to be prominent in PiFM measurements when the thermal expansion of the sample under the tip is significant. It is helpful to establish the lower limit of sample expansion beyond which the PiFM measurement in non-contact mode can no longer register changes to the sample. One way to measure the sensitivity of PiFM to a variable height difference Δz of the sample is illustrated in Figure 17.[15] In this experiment, the sample consists of template-stripped gold (TSG) atop a lead zirconium titanate (PZT) crystal that is periodically modulated at

$f_m = f_2 - f_1$ to mimic the thermally modulated sample expansion. Because of the modulated sample height, we may expect a modulation of the vdW force experienced by the tip. With the tip driven at f_2, the gradient of the modulated tip-sample interaction force can be observed in the f_1 channel, similar to the detection scheme in heterodyne detected PiFM. The measured amplitude change at f_1 is shown in Figure 17(b) as a function of the vibration amplitude Δz of the sample. Operating in non-contact mode, a linear relation is found with a slope of 1 pm/pm. Extrapolation of the linear trend to the noise floor yields a sensitivity limit $\Delta z \sim 32$ pm.

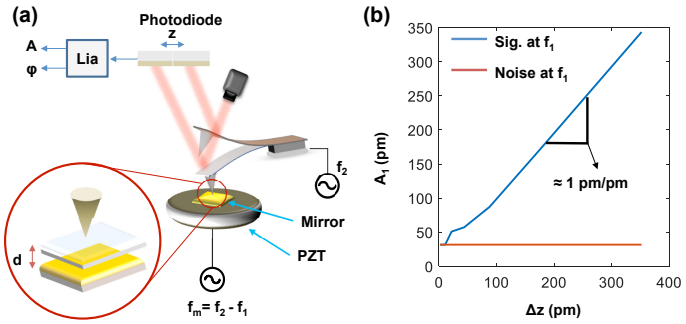

Fig. 17 Sensitivity limit for sensing height variations in a PiFM microscope. (a) Experimental setup. Template-stripped gold attached to a lead zirconium titanate (PZT) crystal is height-modulated at $f_m = f_2 - f_1$ to mimic the thermally modulated expansion. (b) Amplitude change as a function of the sample height variation (blue) and the amplitude noise floor (red). The extrapolated blue curve intersects the noise floor near ~ 32 pm. Reprinted from ref[15] Copyright © 2020.

Sample expansion is a function of the optical power absorbed and the material properties that define how the absorbed power is translated into material expansion. These material properties include the density, specific heat capacity, thermal conductivity and the thermal expansion coefficient of the sample.[37] Since the optical power absorbed is a sensitive function of the sample's absorption coefficient, the thermal diffusivity and the illuminated sample volume, for a given class of materials the latter three parameters often play a crucial role in determining the detectability of thermal effects related to expansion in PiFM experiments.

For instance, several PiFM studies have focused on films of organic polymers under mid-infrared illumination. Photothermal expansion can be expected when the mid-infrared excitation wavelength is tuned into resonance with the molecular vibrational modes of the polymer.

Under typical illumination conditions of a few mW of average power focused onto the sample, the total thermal expansion of a ~ 100 nm layer of polystyrene at its 1492 cm^{-1} resonance is estimated as $\gtrsim 50$ pm, which is higher than the noise floor.[32] The corresponding photo-induced force, in the form of the thermally modulated vdW force, is calculated as a few tens of pN. At the same time, the maximum dipole-dipole electromagnetic force due to the molecular resonance is estimated to be less than a pN. Consequently, a measurement under these conditions is dominated by forces related to thermal expansion of the sample, even when the PiFM experiment is performed in non-contact mode. Since F_{th} grows with the thickness of the sample but the dipole-dipole force is virtually immune to sample thickness beyond the first few molecular layers, thicker layers of the polymer specimen give rise to an even greater contribution from the thermal expansion effect.

An example is shown in Figure 18, which displays PiFM measurements on block co-polymers. When tuning to the 1725 cm^{-1} C=O stretching vibration of PMMA, shown in panel (b), this polymer component gives rise to a strong force due to the photothermal expansion effect. Adjusting the excitation light to 1673 cm^{-1} yields the PiFM image shown panel (c), where the polyvinylpyrrolidone (PVP) component of the blend produces the strongest signal. The spectral dependence of the signal follows the dissipative lineshape of the vibrational resonance, as expected for photothermal forces.[4]

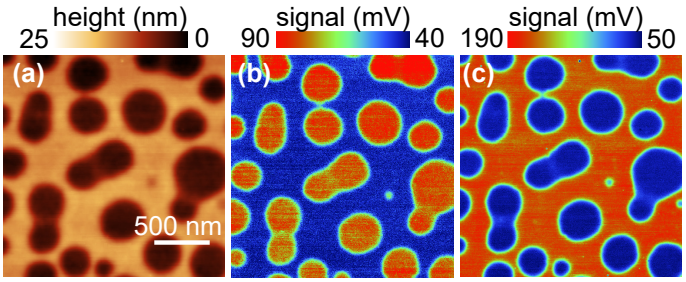

Fig. 18 PiFM on block co-polymers obtained via the harmonic heterodyne detection technique ($n = 1$) with a laser repetition rate of $f_2 - f_1$. (a) Topography of the PVP/PMMA block co-polymer blend. (b) PiFM at 1725cm^{-1} and (c) PiFM at 1673cm^{-1}. The laser repetition rate is fixed at $f_2 - f_1$, where f_1 and f_2 is the first and second mechanical resonance of the cantilever oscillation. Reprinted (adapted) with permission from[4]. Copyright 2019 American Chemical Society

Another way to examine the origin of the signal is to record the PiFM signal as a function of the average tip-sample distance. A PiFM approach curve is displayed in Figure 19 for PMMA on a Si substrate.[14] The red curve shows the response for a bare Si substrate while the blue and black curves show the signals for a 10 nm and a 60 nm thick PMMA layer atop the Si surface. The laser light is tuned to 1735 cm^{-1}, which coincides with the carbonyl vibrational resonance of PMMA. No clear distance dependence of the photo-induced force is seen for bare Si, indicating the absence of either a strong dipole-dipole force or a photothermal expansion force under the current excitation condition. The response from the 10 nm PMMA largely follows the Si curve, underlining that the photothermal expansion for this layer thickness is too small to be registered. For the 60 nm PMMA layer, a clear photo-induced force of a few pN is observed. This force shows a shallow tip-sample distance dependence that can be attributed to photothermal effects. A possible dipole-dipole force, indicated by the green line, would only be evident in the short range. In this case, the expected dipole-dipole force is well below the detection limit and the signal is dominated by forces that originate from thermal expansion.

Both the thermally modulated vdW force and the photoacoustic force are longer range and show dissipative lineshapes. It is useful to examine which force is more dominant in a given experimental scenario. Figure 20 shows the photo-induced force

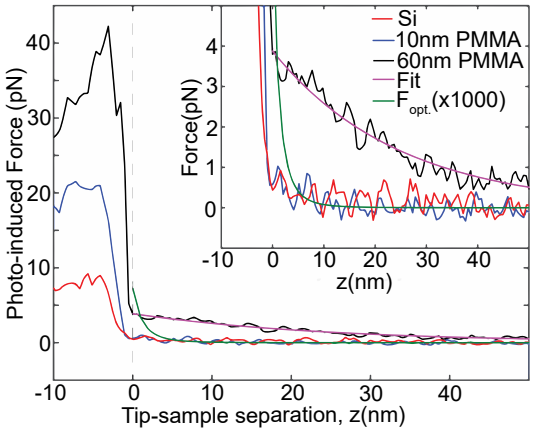

Fig. 19 PiFM approach curve on a bare Si substrate (red), 10 nm PMMA film (blue), 60 nm PMMA film (black), and fit to the 60 nm PMMA curve (purple) at 1735 cm^{-1}. Expected dipole-dipole gradient force is shown in green (multiplied by 10^3. Inset: magnified view in the short tip-sample distance range. Reprinted (adapted) with permission from [14]. Copyright 2018 American Chemical Society

spectrum obtained for a ~ 500 nm thick PMMA sample while the tip is placed ~ 3 μm above the PMMA surface.[15] At such large tip-sample distances, the thermally modulated vdW is negligible, but the photoacoustic forces can still be prominent. At ambient air pressure, a clear vibrational signature of PMMA is seen in the force spectrum, while the force decreases as the air pressure is lowered; strong evidence of the presence of a photoacoutsic response. The shallow tip-sample dependence of the photoacoustic implies it may appear as a near constant background against which other photo-induced forces are measured. In the heterodyne detection mode, however, the photoacoustic contribution is expected to play a only minor role because its gradient is negligible on the nanometer scale.

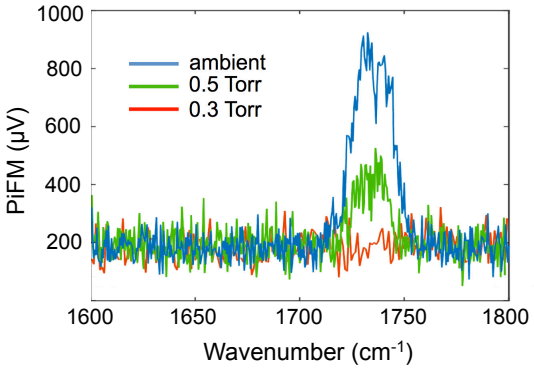

Fig. 20 Photoacoustic response in PiFM obtained from a 500 nm PMMA sample upon infrared excitation at 1733cm^{-1} and a tip-sample distance of $\sim 3\mu m$. Reprinted from ref[15] Copyright © 2020.

4.3 Combination of induced dipole and thermal forces

The induced dipole and the thermal expansion contrast mechanisms can both be relevant in the PiFM measurement. Figure 21 shows a relevant example of an Au nanowire on a glass substrate which is partially covered with a tapered PS layer. The sample is examined in heterodyne AM-PiFM mode with a tip that is covered with a ~ 2 nm thick layer of PDMS, shown schematically in panel 21(a). The schematic of the experiment is shown overlaid with the topography of the sample in Fig. 21(a). Depending on the location in the image and the excitation wavelength, different force mechanisms can contribute to the overall PiFM signal.[32] We will briefly discuss several general features, emphasizing dominant mechanisms over weaker force contributions.

First, when the laser is tuned to 1730 cm^{-1}, none of the materials displays a spectroscopic resonance. In this regime, the force in the region near the exposed Au nanowire is dominated by the electromagnetic force between the tip and the metal wire. Contrast between the glass and the nanowire results from the refractive index differences between the materials, enhanced by the plasmonic gap mode that is only active over the metal wire. The Au nanowire is visible in the exposed areas, but it produces no PiFM signal when buried under the wedged PS material.

The situation is different at 1492 cm^{-1}, where PS has a strong vibrational resonance. Now the PS wedged material is clearly observed in panel (b) via the thermally modulated van der Waals force. The nanowire is visible too. In the exposed area the strongest contribution to the PiFM signal of the nanowire is again the electromagnetic force, whereas under the PS material, the thermal force dominates, benefiting from a moderate enhancement due to the involvement of enhanced fields between the tip and the buried Au nanowire. This gap mode effect disappears as the thickness of the PS layer grows.

At 1268 cm^{-1}, shown in Fig. 21(c), there is a strong vibrational absorption of the PDMS material on the tip. The dominant now is the thermal expansion of the tip at the PDMS resonance, which follows the absorptive Lorentzian shape of the PDMS. This effect is enhanced by the gap mode effect, which produces stronger signals over the Au nanowire. Since the gap mode enhancement becomes weaker with the distance between the tip and the Au nanowire, the signal at 1268 cm^{-1} diminishes as the thickness of the PS wedge grows.

Panel (d) shows the PiFM image at 1020 cm^{-1}. As can be seen in the FTIR spectrum displayed in 21(e), at this vibrational energy both the PDMS and the glass substrate exhibit a resonant response. There is now a strong PiFM signal in the area devoid of PS, as the thermal force above the glass is substantial, in addition to the thermal expansion force introduced by the presence of the PDMS layer on the tip. The thermal glass response rivals the electromagnetic force over the nanowire, offering limited contrast between the glass and the wire in this region.

5 Conclusions

Within a decade after its introduction, the PiFM microscope has matured into a helpful tool for nanoscopic studies with spectroscopic contrast. Several developments have both improved the sensitivity of the approach and expanded its range of applications. At the same time, new insights into the origin of the PiFM signal have contributed to an improved interpretation of the signal. In particular, a better understanding of thermal effects in PiFM has made it possible to more carefully analyze the signal and extract more reliable quantitative information from the mea-

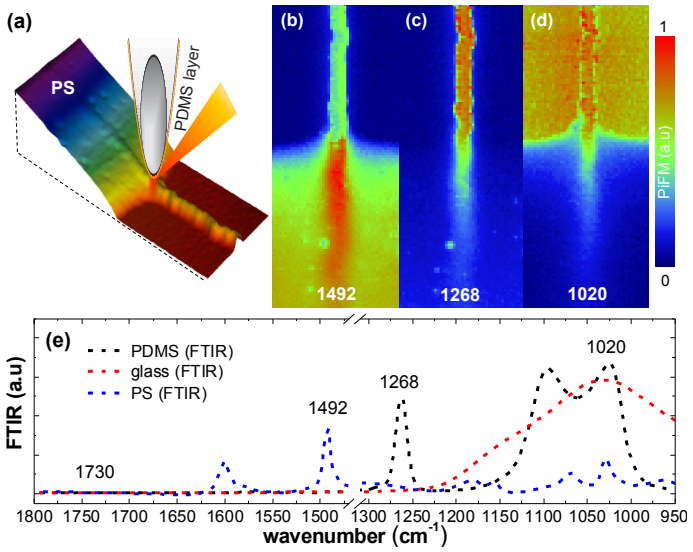

Fig. 21 PiFM imaging of a PS wedge over a Au nanowire on a glass substrate. The tip is covered with a layer of PDMS. (a) Schematic of the experiment overlaid with the topography image. PiFM images taken at (b) 1492 cm^{-1}, (c) 1268 cm^{-1}, and (d) 1020 cm^{-1}, revealing both electromagnetic and thermal forces. (e) FTIR spectra of bulk PS, PDMS and glass in the relevant region of the IR spectrum. Reprinted (adapted) with permission from [32]. Copyright 2019 United States National Academy of Sciences.

surement. These developments are paving the way for an even broader set of applications in years to come.

Conflicts of interest

There are no conflicts to declare.

Acknowledgements

This work was supported by the National Science Foundation, grant CMMI-1905582.

Notes and references

1 I. Rajapaksa, K. Uenal and H. K. Wickramasinghe, Applied physics letters, 2010, **97**, 073121.
2 F. Zenhausern, Y. Martin and H. Wickramasinghe, Science, 1995, **269**, 1083–1085.
3 L. Wang, H. Wang, D. Vezenov and X. G. Xu, The Journal of Physical Chemistry C, 2018, **122**, 23808–23813.
4 L. Wang, D. S. Jakob, H. Wang, A. Apostolos, M. M. Pires and X. G. Xu, Analytical chemistry, 2019, **91**, 13251–13259.
5 H. Wang, E. Janzen, L. Wang, J. H. Edgar and X. G. Xu, Nano letters, 2020, **20**, 3986–3991.
6 I. Rajapaksa and H. Kumar Wickramasinghe, Applied physics letters, 2011, **99**, 161103.
7 J. Jahng, J. Brocious, D. A. Fishman, S. Yampolsky, D. Nowak, F. Huang, V. A. Apkarian, H. K. Wickramasinghe and E. O. Potma, Applied Physics Letters, 2015, **106**, 083113.
8 B. Kim, R. M. Khan, A. Fast, D. A. Fishman and E. O. Potma, The Journal of Physical Chemistry C, 2020, **124**, 11694–11700.
9 J. Yamanishi, Y. Naitoh, Y. Li and Y. Sugawara, Applied Physics Letters, 2017, **110**, 123102.
10 J. Yamanishi, Y. Naitoh, Y. Li and Y. Sugawara, Physical Review Applied, 2018, **9**, 024031.
11 H. Wang, L. Wang, Y. Shang, S. Y. Tafti, W. Cao, Z. Ning, X. F. Zhang and X. G. Xu, Soft Matter, 2020, **16**, 8372–8379.
12 H. U. Yang and M. B. Raschke, New Journal of Physics, 2016, **18**, 053042.
13 F. T. Ladani and E. O. Potma, Physical Review B, 2017, **95**, 205440.
14 B. T. O'Callahan, J. Yan, F. Menges, E. A. Muller and M. B. Raschke, Nano letters, 2018, **18**, 5499–5505.
15 M. A. Almajhadi, S. M. A. Uddin and H. K. Wickramasinghe, Nature communications, 2020, **11**, 1–9.
16 J. Jahng, D. A. Fishman, S. Park, D. B. Nowak, W. A. Morrison, H. K. Wickramasinghe and E. O. Potma, Accounts of chemical research, 2015, **48**, 2671–2679.
17 T. U. Tumkur, X. Yang, B. Cerjan, N. J. Halas, P. Nordlander and I. Thomann, Nano Letters, 2016, **16**, 7942–7949.
18 D. Nowak, W. Morrison, H. K. Wickramasinghe, J. Jahng, E. Potma, L. Wan, R. Ruiz, T. R. Albrecht, K. Schmidt, J. Frommer et al., Science advances, 2016, **2**, e1501571.
19 R. A. Murdick, W. Morrison, D. Nowak, T. R. Albrecht, J. Jahng and S. Park, Japanese Journal of Applied Physics, 2017, **56**, 08LA04.
20 H. K. Wickramasinghe and S. Park, SPIE Newsroom, 2015, 1–3.
21 A. S. Cristie-David, J. Chen, D. B. Nowak, A. L. Bondy, K. Sun, S. I. Park, M. M. Banaszak Holl, M. Su and E. N. G. Marsh, Journal of the American Chemical Society, 2019, **141**, 9207–9216.
22 L. M. Otter, M. W. Förster, E. Belousova, P. O'Reilly, D. Nowak, S. Park, S. Clark, S. F. Foley and D. E. Jacob, Geostandards and Geoanalytical Research, 2021, **45**, 5–27.
23 J. Jahng, J. Brocious, D. A. Fishman, F. Huang, X. Li, V. A. Tamma, H. K. Wickramasinghe and E. O. Potma, Physical Review B, 2014, **90**, 155417.
24 L. Wang, H. Wang, M. Wagner, Y. Yan, D. S. Jakob and X. G. Xu, Science advances, 2017, **3**, e1700255.
25 L. Wang, M. Wagner, H. Wang, S. Pau-Sanchez, J. Li, J. H. Edgar and X. G. Xu, Advanced Optical Materials, 2020, **8**, 1901084.
26 H. Wang, J. M. Gonzalez-Fialkowski, W. Li, Q. Xie, Y. Yu and X. G. Xu, Analytical Chemistry, 2021, **93**, 3567–3575.
27 J. Jahng, E. O. Potma and E. S. Lee, Analytical chemistry, 2018, **90**, 11054–11061.
28 Y. Martin, C. C. Williams and H. K. Wickramasinghe, Journal of applied Physics, 1987, **61**, 4723–4729.
29 J. Jahng, B. Kim, E. S. Lee and E. O. Potma, Physical Review B, 2016, **94**, 195407.
30 T. Albrecht, P. Grütter, D. Horne and D. Rugar, Journal of applied physics, 1991, **69**, 668–673.
31 F. J. Giessibl and M. Tortonese, Applied physics letters, 1997, **70**, 2529–2531.

32 J. Jahng, E. O. Potma and E. S. Lee, Proceedings of the National Academy of Sciences, 2019, **116**, 26359–26366.

33 J. Yamanishi, H. Yamane, Y. Naitoh, Y. J. Li, N. Yokoshi, T. Kameyama, S. Koyama, T. Torimoto, H. Ishihara and Y. Sugawara, Nature Communications, 2021, **12**, 1–7.

34 B. Kim, J. Jahng, A. Sifat, E. S. Lee and E. O. Potma, The Journal of Physical Chemistry C, 2021, **125**, 7276–7286.

35 J. Adamcik, A. Berquand and R. Mezzenga, Applied Physics Letters, 2011, **98**, 193701.

36 A. Dazzi, C. B. Prater, Q. Hu, D. B. Chase, J. F. Rabolt and C. Marcott, Applied spectroscopy, 2012, **66**, 1365–1384.

37 A. Dazzi, F. Glotin and R. Carminati, Journal of Applied Physics, 2010, **107**, 124519.

38 H. Wang, L. Wang, E. Janzen, J. H. Edgar and X. G. Xu, Analytical Chemistry, 2020, **93**, 731–736.

39 L. Novotny and B. Hecht, Principles of nano-optics, Cambridge university press, 2012.

40 J. Jahng, F. T. Ladani, R. M. Khan, X. Li, E. S. Lee and E. O. Potma, Optics letters, 2015, **40**, 5058–5061.

41 A. Ambrosio, M. Tamagnone, K. Chaudhary, L. A. Jauregui, P. Kim, W. L. Wilson and F. Capasso, Light: Science & Applications, 2018, **7**, 1–9.

42 M. Tamagnone, A. Ambrosio, K. Chaudhary, L. A. Jauregui, P. Kim, W. L. Wilson and F. Capasso, Science Advances, 2018, **4**, eaat7189.

43 A. Ambrosio, R. C. Devlin, F. Capasso and W. L. Wilson, ACS Photonics, 2017, **4**, 846–851.

44 F. Lu, M. Jin and M. A. Belkin, Nature photonics, 2014, **8**, 307–312.

45 J. Chae, S. An, G. Ramer, V. Stavila, G. Holland, Y. Yoon, A. A. Talin, M. Allendorf, V. A. Aksyuk and A. Centrone, Nano letters, 2017, **17**, 5587–5594.

46 A. Dazzi and C. B. Prater, Chemical reviews, 2017, **117**, 5146–5173.

47 C.-T. Wang, B. Jiang, Y.-W. Zhou, T.-W. Jiang, J.-H. Liu, G.-D. Zhu and W.-B. Cai, Analytical chemistry, 2019, **91**, 10541–10548.

48 B. Kim and E. O. Potma, Physical Review B, 2019, **100**, 195416.

49 Y. Huang, D. Legrand, R. Vincent, E. A. Dogbe Foli, D. Nowak, G. Lerondel, R. Bachelot, T. Taliercio, F. Barho, L. Cerutti, F. Gonzalez-Posada, B. K. Tay and A. Bruyant, ACS Photonics, 2018, **5**, 4352–4359.

50 T. Shaykhutdinov, A. Furchner, J. Rappich and K. Hinrichs, Opt. Mater. Express, 2017, **7**, 3706–3714.